# Global Uncertainty Propagation and Sensitivity Analysis in the CH 3 OCH 2 + O 2 System: Combining Experiment and Theory To Constrain Key Rate Coefficients in DME Combustion

**ARTICLE** *in* THE JOURNAL OF PHYSICAL CHEMISTRY A · MARCH 2015

Impact Factor: 2.69 · DOI: 10.1021/acs.jpca.5b00620 · Source: PubMed



**6 AUTHORS**, INCLUDING:

Alison Tomlin
University of Leeds
**143** PUBLICATIONS **2,302** CITATIONS
SEE PROFILE

Struan Robertson
Dassault Systemes
**61** PUBLICATIONS **1,384** CITATIONS
SEE PROFILE

Mark A Blitz
University of Leeds
**122** PUBLICATIONS **1,818** CITATIONS
SEE PROFILE

Michael Pilling
University of Leeds
**399** PUBLICATIONS **12,922** CITATIONS
SEE PROFILE

THE JOURNAL OF PHYSICAL CHEMISTRY A

Article

pubs.acs.org/JPCA

# Global Uncertainty Propagation and Sensitivity Analysis in the $CH_3OCH_2 + O_2$ System: Combining Experiment and Theory To Constrain Key Rate Coefficients in DME Combustion

R. J. Shannon,[†] A. S. Tomlin,*[,‡] S. H. Robertson,[§] M. A. Blitz,[†] M. J. Pilling,[†] and P. W. Seakins[†]

[†]School of Chemistry and [‡]Energy Research Institute, School of Chemical and Process Engineering, University of Leeds, Leeds LS2 9JT, U.K.

[§]Dassault Systèmes, BIOVA, Science Park, Cambridge CB4 0WN, U.K.

Supporting Information

**ABSTRACT:** Statistical rate theory calculations, in particular formulations of the chemical master equation, are widely used to calculate rate coefficients of interest in combustion environments as a function of temperature and pressure. However, despite the increasing accuracy of electronic structure calculations, small uncertainties in the input parameters for these master equation models can lead to relatively large uncertainties in the calculated rate coefficients. Master equation input parameters may be constrained further by using experimental data and the relationship between experiment and theory warrants further investigation. In this work, the $CH_3OCH_2 + O_2$ system, of relevance to the combustion of dimethyl ether (DME), is used as an example and the input parameters for master equation calculations on this system are refined through fitting to experimental data. Complementing these fitting calculations, global sensitivity analysis is used to explore which input parameters are constrained by which experimental conditions, and which parameters need to be further constrained to accurately predict key elementary rate coefficients. Finally, uncertainties in the calculated rate coefficients are obtained using both correlated and uncorrelated distributions of input parameters.

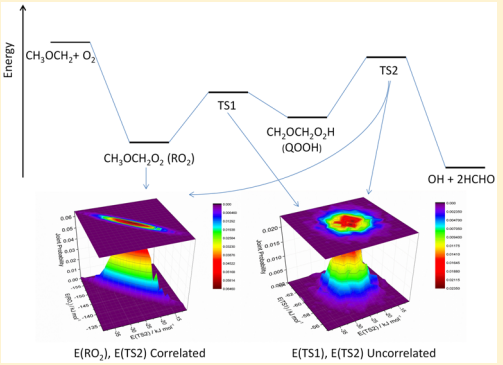


## INTRODUCTION

Theoretical calculations provide a useful way of estimating rate coefficients for systems over wide ranges of temperatures and pressures, some of which are inaccessible from experiments. However, several studies have recently demonstrated that errors, especially in calculated transition state energies, can lead to substantial uncertainties in predicted rate coefficients.[1,2] These uncertainties have been suggested to be from a factor of 2 for simple abstraction reactions[3] up to 5−10 for reactions in complex multiwell systems.[1]

Experimental data can be used to substantially reduce the uncertainties in predicted rate coefficients by constraining the *ab initio* parameters[4,5] and the exploitation of the complementary nature of experiment and theory warrants further exploration. In a recent publication,[6] extensive pulsed photolysis data for the $CH_3OCH_2 + O_2$ reaction were used to constrain the input parameters of a chemical master equation calculation using the implementation of the Levenberg−Marquardt algorithm for parameter optimization within the open source MESMER code.[7] This reaction system is a key step in the combustion of dimethyl ether (DME)[8−13] and, with interest in the use of DME as a possible fuel,[14] the $CH_3OCH_2 + O_2$ reaction has attracted substantial attention.[15−19] The experiments[6] probed the reaction system by observation of OH, formed by dissociation of $CH_2OCH_2OOH$. Both the time dependence of OH formation and its yield were observed. Under the conditions of the experiment, the component of the OH growth associated with chemically activated product was closely related to the time dependence of the loss of $CH_3OCH_2$ by reaction with $O_2$.

In this work, uncertainty propagation and global sensitivity analyses[20−25] are reported for the $CH_3OCH_2 + O_2$ system, first to demonstrate how particular experiments can help to constrain the input parameters to the master equation, and second to explore the causes of remaining uncertainties following the fitting process. These sensitivity analyses were performed both for the conditions of existing experiments and for conditions under which no experimental data are available but which may be important from an applications perspective. This allows the investigation of the relative importance of key parameters that control the uncertainty in rate constant predictions under important combustion conditions, and hence how sensitivity analysis could be used for the purposes

**Special Issue:** 100 Years of Combustion Kinetics at Argonne: A Festschrift for Lawrence B. Harding, Joe V. Michael, and Albert F. Wagner

**Received:** January 21, 2015
**Revised:** March 16, 2015




DOI: 10.1021/acs.jpca.5b00620
J. Phys. Chem. A XXXX, XXX, XXX−XXX

of experimental design. In addition to the sensitivity analysis, we assess the uncertainty in the elementary rate coefficients from the constrained master equation calculations over conditions of relevance to practical devices, using both correlated and uncorrelated input distributions.

## METHODOLOGY

**Master Equation (ME) Calculations.** Figure 1 shows the stationary points on the potential energy surface for the

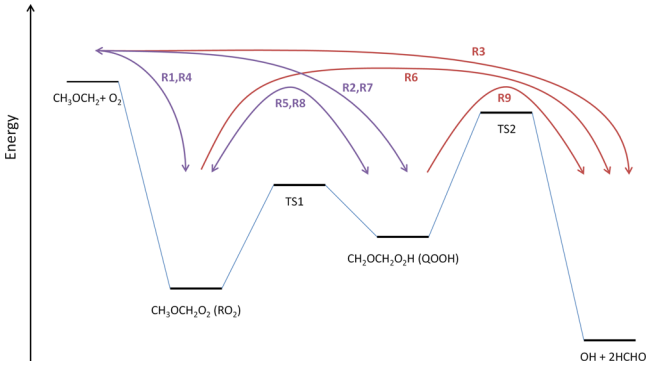


**Figure 1.** Stationary points on the $CH_3OCH_2 + O_2$ potential energy surface from calculations at the CBS-QB3//MPW1K/aug-cc-pVTZ level of theory.[6] $RO_2$ is $CH_3OCH_2O_2$ and QOOH is $CH_2OCH_2OOH$.

$CH_3OCH_2 + O_2$ system. Eskola et al. discussed these energies, obtained from a range of model chemistries, in a recent publication.[6] Although this previous publication found three transition states (TS) leading from QOOH to OH + $2CH_2O$, only the energy of the lowest of these transition states was varied in the fitting calculations, and the energies of the other two TS were scaled such that the difference in energies remained constant. This work utilizes the same approach and the surface in Figure 1 is simplified accordingly. Master equation calculations were performed using the open source MESMER code,[7,26] which has been discussed in a number of recent publications.[13,27] Briefly, the energies of the isomer adducts, $RO_2$ and QOOH, are divided into grains that are used as the basis of the chemical master equation model. The form of the chemical master equation used is

$$\frac{\mathrm{d}}{\mathrm{d}t}\mathbf{p} = \mathbf{M}\mathbf{p} \tag{1}$$

where $\mathbf{p}$ is a vector containing the populations, $p_i(E,t)$, of the energy grains and of the reactants, where $i$ refers to the $i$th isomer, and $\mathbf{M}$ is the matrix that determines grain population evolution due to collisional energy transfer within each isomer and reaction. Reactive processes, which include isomerization between $RO_2$ and QOOH, and dissociation from QOOH, are described by the Rice, Ramsperger, Kassel, and Marcus (RRKM) theory, whereas collisional energy transfer is modeled using an exponential down model parametrized by a temperature dependent $\langle \Delta E \rangle_{\mathrm{down}}$, the average amount of energy transferred in a downward direction upon collision with the bath gas. The temperature dependence is described by the following expression:

$$\langle \Delta E \rangle_{\mathrm{down}} = \langle \Delta E \rangle_{\mathrm{down,ref}} \left( \frac{T}{T_{\mathrm{ref}}} \right)^{d} \tag{2}$$

where $T_{\mathrm{ref}}$ = 298 K. Molecular densities of states were calculated by assuming rigid external rotors and harmonic oscillators, except for those modes best described as internal rotations. Modes corresponding to internal rotations or torsions were modeled as hindered rotations and these modes were projected out of the Hessian matrix according to the method of Sharma et al.[28] The CBS-QB3//MPW1K/aug-cc-pVTZ frequencies, rotational constants, and MPW1K/6-31+G hindrance potentials for internal rotations from Eskola et al.[6] were used in the current study.

For the barrierless association of $CH_3OCH_2$ with $O_2$, microcanonical rate coefficients were calculated using an inverse Laplace transform (ILT) method assuming canonical high pressure limiting rate coefficients of the form

$$k_{\mathrm{a}}(T) = A\left( \frac{T}{T_0} \right)^{n} \exp(-E_{\mathrm{a}}/(k_{\mathrm{B}}T)) \tag{3}$$

where, in the current case, the reference temperature $T_0$ is set to 195 K (the lowest temperature at which experiments were performed) and the activation energy is set to zero in agreement with *ab initio* calculations,[6,29,30] which show the association to be barrierless. The sensitivity of the calculated rate coefficients to the $A$ and $n$ parameters will be explored in the current work. There is only one hydrogen transfer process in this system corresponding to the isomerization between $RO_2$ and QOOH. Tunnelling was treated for this process using an Eckart methodology parametrized using the imaginary frequency of the transition state TS1.[31]

It is important to distinguish between the energy dependent rate coefficients used in the master equation and the pressure and temperature dependent rate coefficients derived from the ME analysis. The former involve passage over a single transition state and are used in microcanonical form. The latter are incorporated in the coupled sets of elementary reactions used in combustion models. They are determined in the MESMER analysis using a method based on an approach developed by Bartis and Widom.[7,32] The resulting elementary reactions are shown in Figure 1. They connect all species, and include so-called well-skipping reactions (e.g., R2, R3, R6) in which the reaction system passes over more than one transition state and avoids stabilization in an intermediate well. These reactions and their associated rate coefficients emerge naturally from the Bartis–Widom analysis; they are most important at lower pressures.

**Uncertainty Propagation and Global Sensitivity Analysis.** The uncertainties in the system parameters used in the master equation analysis were assessed in two ways and global uncertainties within the inputs to the master equation model were propagated using a sampling approach based on a quasi-random set of input samples.[33] For the initial, theory-constrained approach, uncertainty ranges for the input parameters were based on theory calculations alone, and were typical of the type of analysis that might be performed to assist the planning of experiments (see below). A Sobol low discrepancy sequence[33] was chosen for the sampling, because it displays better convergence properties with respect to output statistics than more traditional Monte Carlo pseudo-random sequences. The inputs for each run were sampled from uniform distributions that vary between the upper and lower limits discussed below and given in Table 1. A total of 2048 sample points were sufficient to derive accurate output distributions from the model. The input–output relationships from these


DOI: 10.1021/acs.jpca.5b00620
J. Phys. Chem. A XXXX, XXX, XXX–XXX

**Table 1. Parameter Ranges Used for Sensitivity Analyses[a]**

| | theory-constrained | | experimentally constrained | |
|---|---|---|---|---|
| | lower | upper | lower | upper |
| $E(RO_2)$/kJ mol$^{-1}$ | −149.8 | −141.4 | −159.3 | −132.6 |
| $\langle\Delta E\rangle_{down}$/cm$^{-1}$ | 100.0 | 250.0 | 141.0 | 210.9 |
| $d$ (eq 2) | 0 | 1 | −0.6 | 0.8 |
| ILT $A$ [a] (eq 3) | 0.8 | 2 | 0.9 | 1.2 |
| ILT $n$ (eq 3) | −1.0 | −0.2 | −1.2 | −0.7 |
| $E$(QOOH)/kJ mol$^{-1}$ | −108.8 | −100.4 | −115.5 | −81.5 |
| $E$(TS1)/kJ mol$^{-1}$ | −62.7 | −35.1 | −64.3 | −54.9 |
| $E$(TS2)/kJ mol$^{-1}$ | −29.26 | 8.3 | −38.7 | −10.7 |

[a]The units of the ILT $A$ factor are $10^{-11}$ cm$^3$ molecule$^{-1}$ s$^{-1}$.

samples were subsequently used to perform a global sensitivity analysis using the random sampling high dimensional model representation (RS-HDMR) method.[34] The analysis was performed both for conditions of the proposed experiments and for conditions more typical of those found in combustion devices. In this way it is possible to explore how the key parameters that determine the predictive uncertainty of rate constants calculated for combustion conditions, can be constrained by the proposed experiments.

The first step of the theory-constrained analysis is to assign uncertainty ranges for the parameters used in the master equation modeling as listed in Table 1. Experience from previous systems can be used to estimate these theory-constrained uncertainties but realistically some expert judgment has to be applied. For this work, we have made some use of the results of experimental work to set the parameter ranges. Strictly speaking, this is therefore not a truly a theory-constrained calculation of sensitivity, but in planning experiments, one will generally have some limits on the parameters from either previous studies on the same system or studies of related systems.

The *ab initio* energies at the CBS-QB3 level of theory would usually be expected to exhibit an uncertainty of ∼1 kcal mol$^{-1}$ (4.18 kJ mol$^{-1}$)[3] for stable species, and this uncertainty was used for the energies of $RO_2$ and QOOH. Transition states can be more problematic, and when discussing the *ab initio* calculations in the work of Eskola et al.,[6] the authors pointed out that the transition state TS2 in particular exhibited a large T1 diagnostic of 0.036, which is indicative of multireference effects. The presence of such multireference effects is supported by the fact that a number of high level model chemistries (G4, CBS-Q, CCSD(T)-f12) used in the calculations of Eskola et al.[6] give very different energies for the same species, varying by up to 40 kJ mol$^{-1}$ in the case of TS2. Given the complicated electronic structure in this region of the potential energy surface, it is also possible that other channels exist which were not discovered in the calculations performed by Eskola et al.[6] In view of these observations, larger uncertainty ranges were assigned to the transition state energies.

Because $\langle\Delta E\rangle_{down}$ is usually used as an empirical parameter, its uncertainty is estimated from the typical range of $\langle\Delta E\rangle_{down}$ values with a helium bath gas.[35] Helium is used as the bath gas, because of the availability of more experimental data for this reaction system. Finally, uncertainty ranges for the ILT parameters were assigned on the basis of intuition and upon high pressure limiting association rate coefficients for other R + $O_2$ systems[27] while taking into account existing estimations of the rate coefficient for $CH_3OCH_2$ + $O_2$.[9,11,18]

The fitting of parameters to the experimental data of Eskola et al.[6] was subsequently carried out using the Levenberg−Marquardt nonlinear least-squares fitting routine within MESMER. In the current work, the fits were carried out using the same experimental data as in the work by Eskola et al.,[6] but the additional parameters, $E(RO_2)$, $E$(QOOH), and ILT $A$ were also allowed to vary. In the work of Eskola et al.[6] a detailed comparison was made of both a hindered rotor model and harmonic oscillator only model for the system. Of the two models, the hindered one is the more physically realistic and the differences such a model makes to the fitted parameters has already been discussed in detail. For these reasons only the hindered model is considered in the current work.

The fitting procedure provides experimentally constrained parameter ranges that are independent of the theory-constrained ones and are based on the constraints imposed by the experimental data alone. An ideal situation would be to carry out a third set of calculations incorporating both experimental and theoretical constraints. However, for the current work the aim is to explore the differences between these two different approaches to sensitivity analysis and the different kinds of information that can be obtained. Additionally, for this system, the prevalent multireference effects make it particularly difficult to quantify the theory-constrained uncertainty ranges and in this case, given the extensive experimental data set available, we would emphasize the primacy of the experimental constraints.

Table 1 gives the upper and lower limits on each parameter from a joint probability distribution created using the covariance matrix from the Levenberg−Marquardt fitting. The covariance matrix is provided in the Supporting Information, and the related correlation matrix is given in Table 2. The off-diagonal elements of the correlation matrix $R_{ij}$ are given by

$$R_{ij} = \frac{K_{ij}}{\sigma_i \sigma_j}$$

**Table 2. Correlation Matrix from Levenberg−Marquardt Fits of the Master Equation Input Parameters to the Experimental Data**

| | $E(RO_2)$ | $\langle\Delta E\rangle_{down}$ | $d$ | ILT $A$ | ILT $n$ | $E$(QOOH) | $E$(TS1) | $E$(TS2) |
|---|---|---|---|---|---|---|---|---|
| $E(RO_2)$ | 1 | −0.07 | 0.76 | 0.54 | 0.48 | 0.89 | 0.17 | 0.98 |
| $\langle\Delta E\rangle_{down}$ | −0.07 | 1 | −0.13 | −0.42 | −0.28 | 0.29 | −0.54 | −0.04 |
| $d$ | 0.76 | −0.13 | 1 | 0.23 | 0.16 | 0.52 | −0.15 | 0.86 |
| ILT $A$ | 0.54 | −0.42 | 0.23 | 1 | 0.59 | 0.45 | 0.64 | 0.43 |
| ILT $n$ | 0.48 | −0.28 | 0.16 | 0.59 | 1 | 0.41 | 0.62 | 0.38 |
| $E$(QOOH) | 0.89 | 0.29 | 0.52 | 0.45 | 0.41 | 1 | 0.14 | 0.83 |
| $E$(TS1) | 0.17 | −0.54 | −0.15 | 0.64 | 0.62 | 0.14 | 1 | −0.01 |
| $E$(TS2) | 0.98 | −0.04 | 0.86 | 0.43 | 0.38 | 0.83 | −0.01 | 1 |



DOI: 10.1021/acs.jpca.5b00620
J. Phys. Chem. A XXXX, XXX, XXX−XXX

where $K_{ij}$ are the corresponding elements of the covariance matrix.

These uncertainty ranges are significantly smaller than the proposed theory-constrained uncertainty ranges, for all parameters other than the energy of $CH_3OCH_2O_2$ ($E(RO_2)$) and the energy of $CH_2CH_2OOH$ ($E(QOOH)$). A second global uncertainty propagation and sensitivity analysis was then performed using these experimentally constrained uncertainties to explore how the sensitivities change when the large input ranges of the theory-constrained analysis are altered by the experimental constraints.

The global sensitivity analyses presented in this work utilize an HDMR method,[34,36] as described previously.[1] Briefly the HDMR method uses a hierarchical function expansion to map the relationship between the input parameters $x_1$, ..., $x_n$ and output variables $f(\mathbf{x}) = f(x_1, ..., x_n)$ of a model as follows:

$$f(\mathbf{x}) = f_0 + \sum_{i=1}^{n} f_i(x_i) + \sum_{1\le i<j\le n} f_{ij}(x_i,x_j) \tag{4}$$

Here, we applied random sampling HDMR (RS-HDMR), where the functions $f_i(x_i)$ and $f_{ij}(x_i,x_j)$ in (4) are approximated by orthonormal polynomials fitted using a quasi-random sample of full model runs:

$$f_i(x_i) \approx \sum_{r=1}^{k} \alpha_r^i \varphi_r(x_i)$$

$$f_{ij}(x_i,x_j) \approx \sum_{p=1}^{l}\sum_{q=1}^{l'} \beta_{pq}^{ij} \varphi_p(x_i)\,\varphi_q(x_j) \tag{5}$$

where $k$, $l$, and $l'$ represent the order of the polynomial expansion, $\alpha_r^i$ and $\beta_{pq}^{ij}$ are constant coefficients, and $\varphi_r(x_i)$, $\varphi_p(x_i)$, and $\varphi_q(x_j)$ are the orthonormal basis functions. For given input parameter ranges, the sensitivity indices indicate the relative contribution of each parameter to the predicted output variance and can be used to explore interactions between parameters. To compute the sensitivity indices, the partial variances $D_i$ and $D_{ij}$ are calculated from the expansion coefficients:

$$D_i = \sum_{r=1}^{k_i} (\alpha_r^i)^2$$

$$D_{ij} = \sum_{p=1}^{l_i}\sum_{q=1}^{l_j'} (\beta_{pq}^{ij})^2 \tag{6}$$

Finally, the sensitivity indices are calculated from $S_i = D_i/D$, $S_{ij} = D_{ij}/D$, where $D$ is the total variance[37] given by

$$D = \int_{K^n} f^2(x)\,\mathrm{d}x - f_0^2 \tag{7}$$

where $K^n = \{(x_1, ..., x_n), i = 1, ..., n\}$ represents an integral across the unit hypercube represented by the input Sobol sample. For the correlated experimentally constrained sample, marginal indices are obtained as explained further in the results section.

The experimental data available for the $CH_3OCH_2 + O_2$ reaction consist of OH yields and rate coefficients for the overall loss of $CH_3OCH_2$ for temperatures between 195 and 650 K and pressures from $5 \times 10^2$ to $5 \times 10^4$ Pa. However, key quantities of interest to the combustion community are rate coefficients for the elementary processes involved in the reaction. To reflect this, the sensitivity analyses have also been carried out using a number of the predicted elementary rate coefficients as outputs over a wider range of temperatures and pressures than covered by the experimental conditions. The purpose here is to establish how the errors in predicted rate coefficients from the constrained model, extrapolate to conditions of interest for modeling practical devices. The phenomenological reactions (R1−R9) needed for a combustion model are shown in Figure 1 and are listed below.

$$CH_3OCH_2 + O_2 \rightarrow CH_3OCH_2O_2 \quad (R1)$$

$$CH_3OCH_2 + O_2 \rightarrow CH_2OCH_2O_2H \quad (R2)$$

$$CH_3OCH_2 + O_2 \rightarrow OH + 2CH_2O \quad (R3)$$

$$CH_3OCH_2O_2 \rightarrow CH_3OCH_2 + O_2 \quad (R4)$$

$$CH_3OCH_2O_2 \rightarrow CH_2OCH_2O_2H \quad (R5)$$

$$CH_3OCH_2O_2 \rightarrow OH + 2CH_2O \quad (R6)$$

$$CH_2OCH_2O_2H \rightarrow CH_3OCH_2 + O_2 \quad (R7)$$

$$CH_2OCH_2O_2H \rightarrow CH_3OCH_2O_2 \quad (R8)$$

$$CH_2OCH_2O_2H \rightarrow OH + 2CH_2O \quad (R9)$$

**Generation of Joint Probability Distribution.** The provision of confidence limits on the master equation observables for use by the modeling community is particularly important for the elementary rate coefficients that have not been directly validated by experiments. Confidence limits can be obtained by propagating errors described by the input distributions with experimentally constrained ranges from Table 1 and should take into account correlations between parameters that result from the fitting. Joint probability distributions, accounting for correlations, were obtained as described in Kucherenko et al.[38] A Sobol sequence was first transformed into a standard normal vector $\tilde{\mathbf{x}}$ with zero mean and unit variance using the inverse normal cumulative distribution function. A Cholesky decomposition of the covariance matrix, $\boldsymbol{\Sigma}$, from the Marquardt fitting was then calculated:

$$\boldsymbol{\Sigma} = \mathbf{A}\mathbf{A}^{\mathrm{T}} \tag{8}$$

and a joint probability distribution of the parameters $\mathbf{x}$ was obtained from $\tilde{\mathbf{x}}$ as follows:

$$\mathbf{x} = \mathbf{A}\tilde{\mathbf{x}} + \boldsymbol{\mu} \tag{9}$$

Here $\boldsymbol{\mu}$ is a vector of the mean values for each parameter where each element $\mu_i$ is the mean value for parameter $i$ taken from the Marquardt fitting procedure. The full covariance matrix is available in the Supporting Information.

Using the joint probability distribution, uncertainty parameters, $f$, were obtained for reactions R1−R9 as follows:[39]

$$f = \log_{10}\left(\frac{k^{\mu} + 3\sigma}{k^{\mu}}\right) \tag{10}$$

where is $k^{\mu}$ the mean value of a given rate coefficient and $\sigma$ is the standard deviation in the rate coefficient taken from the output distribution. The rate coefficient $k$ can then be described as uncertain according to a multiplicative factor of $10^f$.



DOI: 10.1021/acs.jpca.5b00620
J. Phys. Chem. A XXXX, XXX, XXX−XXX

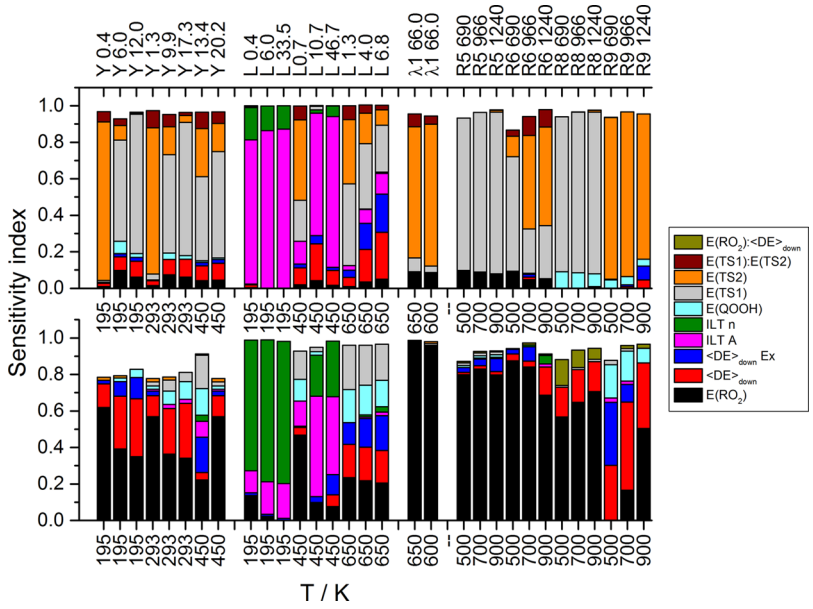


**Figure 2.** Sensitivity indices for the parameters involved in the master equation modeling with theory-constrained parameter ranges (top) and experimentally constrained parameter ranges (bottom). The labels on the top axis give the pressure at which the calculations were run in kPa and identify the type of observable: *Y* indicates the OH yield, *L* indicates the rate coefficient for $CH_2OCH_3$ loss, $\lambda 1$, indicates the time constant corresponding to the longer time formation of OH and *R* indicates a particular elementary rate coefficient. Where the sensitivities sum to be significantly less than 1, this can be attributed to contributions from the second-order sensitivities that are not included. Where there is a colon between two parameters, this indicates a second-order sensitivity for this pair of inputs.

## RESULTS

**Theory-Constrained Analysis.** Using the theory-constrained ranges in conjunction with a Sobol sequence, we obtained distributions for the different rate coefficients and yields calculated with MESMER. Given the necessarily large ranges assigned, it is not surprising that these distributions are wide, with *f* values up to 1.3 (i.e., uncertainties of up to a factor of 20). First- and second-order sensitivities for all eight parameters as listed in Table 1 were obtained using RS-HDMR. These are shown in the upper panel of Figure 2 for OH yields (*Y*) and $CH_3OCH_2$ loss rates (*L*) for a range of conditions. Mittal et al.[11] identified the elementary rate coefficients for reaction R9 (QOOH decomposition to OH + $2CH_2O$) and reaction R5 ($RO_2$ → QOOH isomerization) to be particularly important in the low temperature combustion of DME, and Figure 2 also shows the sensitivities for these two elementary rate coefficients at 500, 700, and 900 K. In addition, the sensitivities for the elementary rate coefficients of reactions R6 (decomposition of $RO_2$ to OH + $2CH_2O$) and R8 (isomerization of QOOH back to $RO_2$) are also shown. Only the first-order and the major second-order indices are shown here and hence the total indices ($\sum S_i + \sum S_{i,j}$) may be less than unity in some cases.

Considering the yields, it was found that the two transition state energies *E*(TS1) (gray bars) and *E*(TS2) (orange bars) give the largest contributions to the predicted variance, through high first-order sensitivities and also via a large contribution from the second-order interaction term. As the pressure is decreased, the first-order sensitivity index for *E*(TS2) increases and that for *E*(TS1) decreases concomitantly. The large second-order sensitivity is likely due to the fact that the uncertainty ranges for *E*(TS1) and *E*(TS2) are close to overlapping. These high sensitivities for *E*(TS1) and *E*(TS2) suggest that experimental measurements of the yields would provide a high level of constraint on these two parameters, and this is reflected to some extent in Table 1 that shows that the post experimental uncertainty range for TS1 is significantly smaller than that for the other energies.

Turning to the theory-constrained sensitivities of the $CH_2OCH_3$ loss rate, the ILT parameters *A* (pink bars) and, to a lesser extent, *n* (green bars) dominate the sensitivities at lower temperatures. At 650 K, the rate coefficients are more sensitive to *E*(TS1), *E*(TS2), and the energy transfer parameters.

Given the large theory-constrained uncertainty ranges for *E*(TS1) and *E*(TS2), it is these parameters that again dominate the sensitivities for the elementary rate coefficients, as shown in the right-hand panel in Figure 2. For the decomposition rate coefficients (R6 and R9) it is found that *E*(TS2) is the dominant parameter because TS2 is the main bottleneck to product formation. Conversely *E*(TS1) dominates the sensitivities for the two isomerization steps R5 and R8. Because the transition state energies dominate the uncertainty in both the OH yields and important rate constant estimations, this suggests that measuring OH yields is critical to constraining the rate constants. Further constraints on these transition states are also provided by measurements of $CH_2OCH_3$ loss rates at higher temperatures. This sensitivity information therefore gives important information that could be used in optimizing experimental design.

In addition to yields and loss rates, experimental reciprocal time constants for OH formation on a longer time scale are available from the work of Eskola et al.,[6] and these correspond to the eigenvalue $\lambda_1$ from the master equation analysis in the 600 to 650 K regime. These time constants are associated with OH formation from the thermalized $RO_2$ species and from Figure 2 it can be seen that $E(TS_2)$ dominates the sensitivities for these eigenvalues at both 650 and 600 K. This is understandable because TS2 is the dominant bottleneck for this process. There is also some sensitivity displayed to


DOI: 10.1021/acs.jpca.5b00620
J. Phys. Chem. A XXXX, XXX, XXX−XXX

$E(RO_2)$; however, this is less significant than in the $E$(TS2) case due to the much larger uncertainty range on $E$(TS2).

**Experimentally Constrained Analysis.** The theory-constrained sensitivity analysis supports our previous work[6] in demonstrating that, despite the complications surrounding the *ab initio* calculation of the barrier heights, the energies of the two transition states, TS1 and TS2, can be well constrained by fitting master equations calculations for $CH_3OCH_2 + O_2$ to the available experimental data. This is demonstrated by the experimentally constrained uncertainty ranges given in Table 1 for $E$(TS1) and $E$(TS2), which are significantly narrower than the theory-constrained values. In the current work, all eight parameters were defined through the Marquardt fitting procedure, but we show that $E$(QOOH) is the least well-defined with an experimentally constrained uncertainty range of 34 kJ mol$^{-1}$ (Table 1).

A second set of sensitivity analyses was performed using the experimentally constrained uncertainty ranges in Table 1, allowing investigation of the causes of the remaining uncertainty in the predictions from the master equation model. In the experimentally constrained case, the covariance matrix from the Marquardt calculations was used to create joint probability distributions as described above. The marginal sensitivities for this correlated sample are shown in Figure 2 (lower panel). These have again been calculated using RS-HDMR but in this case, because correlations are present, the ordering of parameters within the transformations described in eqs 8 and 9 affects the marginal sensitivities. Although this complicates the interpretation of the sensitivity indices somewhat, ignoring correlations would lead to the decomposition of an artificially high output variance and hence, though simpler to interpret, would give misleading results. For the interpretation of marginal indices resulting from parameter correlations we follow the method of Mara and Tarantola.[40] The sensitivity indices shown correspond to the full $S_i$ for $E(RO_2)$ including its correlated effects, the marginal $S_i$ for $\langle\Delta E\rangle_{down}$ without its correlative contribution with $E(RO_2)$, the marginal $S_i$ for ILT $A$ without its correlative contribution with $E(RO_2)$ and $\langle\Delta E\rangle_{down}$ and so on, following the order given in Table 1. A full variance decomposition for correlated inputs providing all marginal indices requires all permutations of the Cholesky decomposition to be used, which is beyond the scope of this paper. However, the marginal sensitivities for the ordering used here still provide useful information that should be interpreted along with information from the covariance matrix.[40]

Figure 2 shows that the energies of the two transition states no longer dominate the sensitivities in the experimentally constrained analysis. The yields now show large sensitivity indices for $E(RO_2)$ (black bars) in particular, and also for $\langle\Delta E\rangle_{down}$ (red bars) with the marginal sensitivity for $E$(TS1) now only becoming important at high temperatures and low pressures. The predicted loss rates for $CH_3OCH_2$ are again dominated by ILT parameters at low temperatures but with the temperature exponent, $n$, now the more important. $E$(TS1) has large sensitivity indices at higher temperatures. It should be noted that $E(RO_2)$ and $E$(TS2) are strongly correlated as shown in Figure 3 and Table 2, and hence, a strong sensitivity to $E(RO_2)$ also implies some sensitivity to $E$(TS2). The same arguments can be applied to other input parameters that are highly correlated and the full correlation matrix obtained from the covariance matrix (Table 2) indicated a high level of

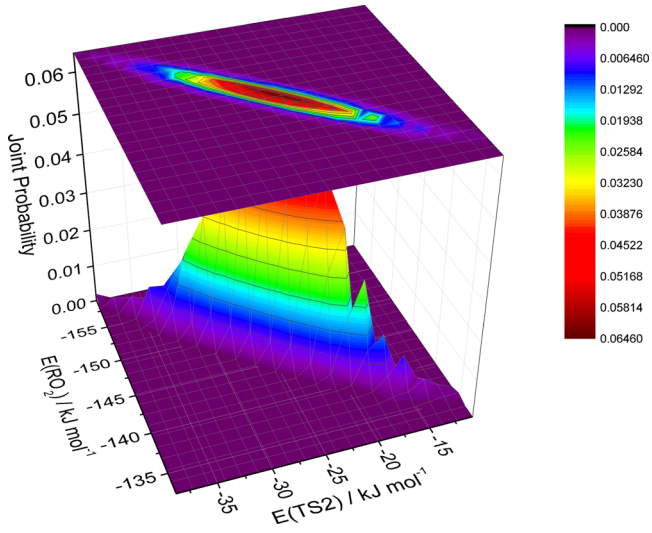


**Figure 3.** Joint probability distributions for $E$(TS2) and $E(RO_2)$ for which the correlation matrix element is 0.98.

correlation between the energies $E(RO_2)$, $E$(QOOH) (cyan bars), and $E$(TS2).

For the elementary rate coefficients, $E(RO_2)$ is again the dominant parameter followed by $\langle\Delta E\rangle_{down}$. These elementary rate coefficients are predominantly sensitive to the equilibrium constant between $RO_2$ and QOOH. However, when the experimentally constrained parameter ranges and correlations for the current sample are used, it is $E(RO_2)$ that has the largest sensitivity index in the majority of cases, although it is strongly correlated to $E$(QOOH). The elementary rate coefficient for reaction R9, the unimolecular decomposition of the QOOH to form $2CH_2O + OH$, exhibits the largest marginal sensitivity indices for $E$(QOOH), and this is most constrained by the higher temperature measurements of $CH_3OCH_2$ loss rates.

In the case of the eigenvalues $\lambda_1$ it is found that $E(RO_2)$ almost entirely dominates the sensitivities. For these eigenvalues it is the energy gap between $E(RO_2)$ and $E$(TS2) that would be expected to be the most important parameter and given that the postexperimental uncertainty range for $E(RO_2)$ is larger than that for $E$(TS2), it is not surprising the $E(RO_2)$ displays the largest sensitivity indices; however, the extent to which this parameter dominates is exacerbated by the fact that $E$(TS2) is strongly correlated to $E(RO_2)$ and thus, as noted above, the $E(RO_2)$ sensitivities could also imply sensitivity to $E$(TS2).

From an experimental perspective, it is observables such as yields or total loss rates that are the most amenable to measurement. However, although they are not measured directly, it is the elementary rate coefficients that are of most interest to the combustion modeling community. Fitting input parameters to experiment is a vital tool in statistical rate theory, allowing the predicted elementary rate coefficients to be constrained by the available experimental quantities. In view of this, sensitivity analysis for the data presented here for the experimentally determined variables should be interpreted slightly differently from that for the elementary rate coefficients. The sensitivity analysis data for the yields and total loss rate give information regarding which experimental conditions can be used to constrain which parameters, whereas the sensitivity data for the elementary reactions demonstrate which parameters need to be further constrained to reduce the


DOI: 10.1021/acs.jpca.5b00620
J. Phys. Chem. A XXXX, XXX, XXX−XXX

Table 3. Uncertainty Parameters $f$ from Both Correlated (C Bold) and Uncorrelated (U) Distributions[a]

| | 500 K, 6.9 × $10^1$ kPa | | 500 K, 6.9 × $10^3$ kPa | | 700 K, 9.6 × $10^1$ kPa | | 700 K, 9.7 × $10^3$ kPa | | 900 K, 1.2 × $10^2$ kPa | | 900 K, 1.2 × $10^4$ kPa | |
|---|---|---|---|---|---|---|---|---|---|---|---|---|
| | **C** | U | **C** | U | **C** | U | **C** | U | **C** | U | **C** | U |
| R1 | **0.11** | 0.10 | **0.13** | 0.11 | **0.10** | 0.16 | **0.17** | 0.15 | **0.12** | 0.24 | **0.19** | 0.17 |
| R2 | **0.34** | 0.41 | **0.28** | 0.37 | **0.36** | 0.41 | **0.28** | 0.39 | **0.35** | 0.39 | **0.28** | 0.39 |
| R3 | **0.19** | 0.39 | **0.47** | 0.61 | **0.15** | 0.30 | **0.37** | 0.52 | **0.11** | 0.23 | **0.34** | 0.46 |
| R4 | **0.71** | 0.67 | **0.72** | 0.69 | **0.55** | 0.49 | **0.59** | 0.54 | **0.47** | 0.38 | **0.51** | 0.44 |
| R5 | **0.64** | 0.71 | **0.65** | 0.71 | **0.54** | 0.55 | **0.52** | 0.55 | **0.50** | 0.48 | **0.45** | 0.46 |
| R6 | **0.44** | 0.81 | **0.66** | 0.74 | **0.24** | 0.58 | **0.31** | 0.66 | **0.18** | 0.46 | **0.23** | 0.53 |
| R7 | **0.92** | 0.72 | **0.89** | 0.80 | **0.76** | 0.59 | **0.71** | 0.62 | **0.65** | 0.47 | **0.60** | 0.52 |
| R8 | **0.73** | 0.73 | **0.73** | 0.73 | **0.60** | 0.57 | **0.58** | 0.59 | **0.53** | 0.44 | **0.50** | 0.49 |
| R9 | **0.45** | 0.81 | **0.50** | 0.92 | **0.31** | 0.56 | **0.37** | 0.66 | **0.30** | 0.43 | **0.28** | 0.51 |

[a]For the uncorrelated distributions, the off-diagonal elements of the covariance matrix were assigned as zero.

uncertainty in these calculated values. The combination of the two sets of sensitivity data provides vital insights into how experiments can be designed to best reduce uncertainties in estimated rate constants under conditions of relevance to combustion simulations. The experimental results of Eskola et al.[6] constrain the key parameters $E(RO_2)$ and $E(QOOH)$ relatively poorly, because they are largely confined to low temperatures and relatively low pressures. The present results show that more extensive experimental data at 500 K and above would constrain these parameters further, and hence the rate coefficients for the key elementary reactions would be constrained more fully.

**Uncertainty Factors for Elementary Rate Coefficients.** Uncertainty parameters were obtained from both the correlated and uncorrelated experimentally constrained distributions to estimate errors in the rate coefficients calculated using MESMER (Table 3). For the uncorrelated distributions all off-diagonal terms in the covariance matrix were set to zero, purely for comparison purposes. The extent of the correlation between some parameters is shown in the joint probability distributions in Figures 3 and 4. These correspond to one pair of parameters that are highly correlated and one pair of parameters that are relatively independent with correlation matrix elements of +0.98 and −0.01 for $E(RO_2)$ and $E(TS2)$ and for $E(TS2)$ and $E(TS1)$, respectively. These results highlight the importance of taking account of correlations between the fitted parameters in order not to overestimate the uncertainty factors. The analysis supports previous findings by Nagy and Turányi concerning the treatment of correlations in the uncertainty parameters for Arrhenius expressions.[41−43] The correlations will also affect the interpretation of the sensitivity information as highlighted above. A high total sensitivity to $E(RO_2)$ or $E(TS2)$ will lead to a high sensitivity in the other because of their high correlation.

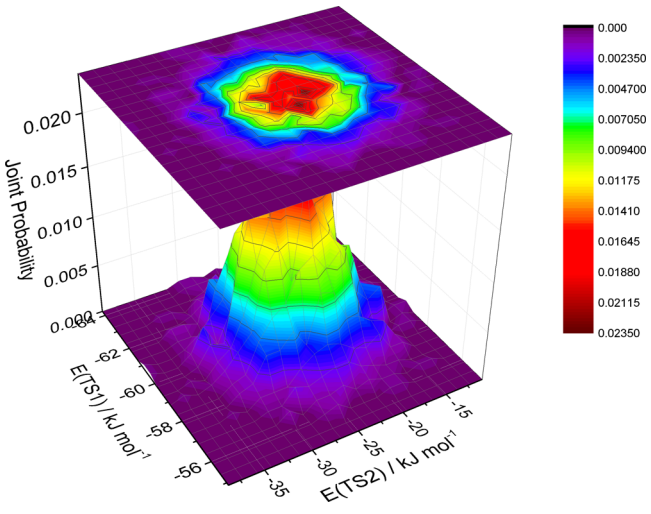


Figure 4. Joint probability distributions for $E(TS1)$ and $E(TS2)$ for which the correlation matrix element is −0.01.

The uncertainties from the correlated sample in Table 3 show substantial reductions of up to a factor of 2 when compared to the corresponding ones from the uncorrelated sample. Under conditions typical of combustion applications (700, 900 K and 970, 1200 kPa), the uncertainty of the rate constant for the isomerization reaction $RO_2 \rightarrow QOOH$ has an $f$ factor of approximately 0.5, which implies uncertainties of around a factor of 3. The rate constant for $QOOH \rightarrow OH + 2CH_2O$ has a lower uncertainty that corresponds to around a factor of 2 for typical combustion conditions. Both of these reactions were highlighted as being extremely sensitive for low temperature predictions of DME combustion in both flow reactors and ignition studies by Tomlin et al.[44] Thus, providing better quantification of these rates is important for improving the robustness of low temperature combustion simulations of DME. Well skipping reactions develop naturally from the Bartis−Widom analysis of the master equation in the present study but have not been included in DME oxidation mechanisms to date. These reactions are fairly well constrained by the current study with uncertainties of a factor of 2 or lower. The current study therefore provides useful data for the improvement of DME oxidation mechanisms. The highest remaining uncertainties are for $QOOH \rightarrow RO_2$, which directly affects the lifetime and concentration of QOOH and hence the rate of branching in combustion systems, particularly at the lower temperatures. This may result from the poor constraint of $E(QOOH)$ by the current experiments.

## CONCLUSIONS

1. We have demonstrated that the large amount of pulsed photolysis data available for the $CH_3OCH_2 + O_2$ reaction can be used to constrain many of the key parameters used in master equation modeling of the system. Sensitivity analysis using proposed theory-constrained uncertainties supports our previous work in demonstrating how accurate experimental data can constrain *ab initio* transition state energies in multiwell systems.

2. Repeating the sensitivity analyses with correlated samples from the Marquardt fitting to the pulsed photolysis results highlights which model parameters are constrained by which


DOI: 10.1021/acs.jpca.5b00620
J. Phys. Chem. A XXXX, XXX, XXX−XXX

experiments, and which parameters are important in the determination of key elementary rate coefficients.

3. The low temperature experiments probing the time dependence of OH formation, and hence the loss of $CH_3OCH_2$, were particularly successful in constraining the ILT parameters for the initial reaction of $CH_3OCH_2$ with $O_2$. One important observation from both the theory and experimentally constrained analyses is that in both cases the low temperature loss rates are dominated by the ILT parameters. Quantities other than the loss rates display negligible sensitivities to these parameters, and this demonstrates how an ILT method can be effectively parametrized by experimental measurements of loss rates even in cases where the high pressure limit has not yet been achieved.

4. Referring to the theory-constrained analyses, the sensitivity indices for the OH yield experiments suggest that these data successfully constrain the energies of TS1 and TS2. The reduced theory-constrained uncertainty ranges for these parameters compared to $E$(QOOH) and $E(RO_2)$ support this observation. Through constraints on $E$(TS1) and $E$(TS2) these experiments reduce uncertainties in predicted rate coefficients for the decomposition reactions of QOOH and $RO_2$ to OH + $2CH_2O$, particularly at higher temperatures.

5. Fits to the experimental data were less successful in constraining energies for $RO_2$ and QOOH, although post experiment analyses show high sensitivity to $E(RO_2)$. The energy of QOOH, which is important in branching steps in low temperature combustion, is poorly constrained by the experimental data available.

The key elementary rate coefficients, as shown in the right-hand panels in Figure 2 appear more sensitive to $E(RO_2)$ than $E$(QOOH). However, there are strong correlations between $E(RO_2)$, $E$(TS2), and $E$(QOOH) (Table 2), which may imply strong joint sensitivities.

6. Given the importance of QOOH in low temperature combustion, the low marginal sensitivity to $E$(QOOH) and $E$(TS2) shown in the post experiment analysis demonstrate the need for a wider range of experimental conditions. $E$(QOOH) is most sensitive to experiments at higher temperatures, via the loss rates of $CH_3OCH_2$ in particular. However, through its correlation with $E(RO_2)$, as discussed above, this parameter is still likely to influence rate constant predictions. By performing experiments across a range of temperatures and pressures, we could further constrain the marginal effects of these two parameters because $E(RO_2)$ dominates for lower temperature OH yields and $E$(QOOH) for higher temperature $CH_3OCH_2$ loss rates. $E(RO_2)$ is particularly sensitive to $\lambda_1$ and experiments over a range of temperatures should provide improved constraints.

7. In addition to the sensitivity analysis, the work demonstrates the importance of accounting for correlations between input parameters when predictive errors are estimated, because otherwise the uncertainties on theoretically predicted rate coefficients can be substantially overestimated. The remaining uncertainties within the constrained master equation model for two key elementary reaction rate coefficients were found to be between factors of 1.3 and 3.5 depending upon the conditions.

## ■ ASSOCIATED CONTENT

### Supporting Information

A table detailing the covariance matrix from the Levenberg–Marquardt fitting is available in Supporting Information. This material is available free of charge via the Internet at http://pubs.acs.org

## ■ AUTHOR INFORMATION

### Corresponding Author

*E-mail: A.S.Tomlin@leeds.ac.uk. Tel: +44 113 3432500.

### Notes

The authors declare no competing financial interest.

## ■ ACKNOWLEDGMENTS

The authors acknowledge the EPSRC (grant EP/J010871/1) for funding.

## ■ REFERENCES

(1) Goldsmith, C. F.; Tomlin, A. S.; Klippenstein, S. J. Uncertainty Propagation in the Derivation of Phenomenological Rate Coefficients from Theory: A Case Study of N-Propyl Radical Oxidation. *Proc. Combust. Inst.* **2013**, *34*, 177–185.

(2) Klippenstein, S. J.; Harding, L. B.; Davis, M. J.; Tomlin, A. S.; Skodje, R. T. Uncertainty Driven Theoretical Kinetics Studies for $CH_3OH$ Ignition: $HO_2$+$CH_3OH$ and $O_2$+$CH_3OH$. *Proc. Combust. Inst.* **2011**, *33*, 351–357.

(3) Curtiss, L. A.; Redfern, P. C.; Raghavachari, K. Assessment of Gaussian-4 Theory for Energy Barriers. *Chem. Phys. Lett.* **2010**, *499*, 168–172.

(4) Prager, J.; Najm, H. N.; Zador, J. Uncertainty Quantification in the *Ab Initio* Rate-Coefficient Calculation for the $CH_3CH(OH)CH_3$ + OH -> $CH_3C(OH)CH_3$ + $H_2O$ Reaction. *Proc. Combust. Inst.* **2013**, *34*, 583–590.

(5) Burke, M. P.; Klippenstein, S. J.; Harding, L. B. A Quantitative Explanation for the Apparent Anomalous Temperature Dependence of OH + $HO_2$ = $H_2O$ + $O_2$ through Multi-Scale Modeling. *Proc. Combust. Inst.* **2013**, *34*, 547–555.

(6) Eskola, A. J.; Carr, S. A.; Shannon, R. J.; Wang, B.; Blitz, M. A.; Pilling, M. J.; Seakins, P. W.; Robertson, S. H. Analysis of the Kinetics and Yields of OH Radical Production from the $CH_3OCH_2$ + $O_2$ Reaction in the Temperature Range 195–650 K: An Experimental and Computational Study. *J. Phys. Chem. A* **2014**, *118*, 6773–6788.

(7) Glowacki, D. R.; Liang, C. H.; Morley, C.; Pilling, M. J.; Robertson, S. H. MESMER: An Open-Source Master Equation Solver for Multi-Energy Well Reactions. *J. Phys. Chem. A* **2012**, *116*, 9545–9560.

(8) Zador, J.; Taatjes, C. A.; Fernandes, R. X. Kinetics of Elementary Reactions in Low-Temperature Autoignition Chemistry. *Prog. Energy Combust. Sci.* **2011**, *37*, 371–421.

(9) Curran, H. J.; Fischer, S. L.; Dryer, F. L. The Reaction Kinetics of Dimethyl Ether. II: Low-Temperature Oxidation in Flow Reactors. *Int. J. Chem. Kinet.* **2000**, *32*, 731–759.

(10) Curran, H. J.; Pitz, W. J.; Westbrook, C. K.; Dagaut, P.; Boettner, J. C.; Cathonnet, M. A Wide Range Modeling Study of Dimethyl Ether Oxidation. *Int. J. Chem. Kinet.* **1998**, *30*, 229–241.

(11) Mittal, G.; Chaos, M.; Sung, C. J.; Dryer, F. L. Dimethyl Ether Autoignition in a Rapid Compression Machine: Experiments and Chemical Kinetic Modeling. *Fuel Process. Technol.* **2008**, *89*, 1244–1254.

(12) Bansch, C.; Kiecherer, J.; Szori, M.; Olzmann, M. Reaction of Dimethyl Ether with Hydroxyl Radicals: Kinetic Isotope Effect and Prereactive Complex Formation. *J. Phys. Chem. A* **2013**, *117*, 8343–8351.

(13) Carr, S. A.; Still, T. J.; Blitz, M. A.; Eskola, A. J.; Pilling, M. J.; Seakins, P. W.; Shannon, R. J.; Wang, B.; Robertson, S. H. Experimental and Theoretical Study of the Kinetics and Mechanism of the Reaction of OH Radicals with Dimethyl Ether. *J. Phys. Chem. A* **2013**, *117*, 11142–11154.

(14) Ribeiro, N. M.; Pinto, A. C.; Quintella, C. M.; da Rocha, G. O.; Teixeira, L. S. G.; Guarieiro, L. L. N.; Rangel, M. D.; Veloso, M. C. C.; Rezende, M. J. C.; da Cruz, R. S.; et al. The Role of Additives for



DOI: 10.1021/acs.jpca.5b00620
J. Phys. Chem. A XXXX, XXX, XXX–XXX

Diesel and Diesel Blended (Ethanol or Biodiesel) Fuels: A Review. *Energy Fuels* **2007**, *21*, 2433−2445.
(15) Maricq, M. M.; Szente, J. J.; Hybl, J. D. Kinetic Studies of the Oxidation of Dimethyl Ether and Its Chain Reaction with $Cl_2$. *J. Phys. Chem. A* **1997**, *101*, 5155−5167.
(16) Rosado-Reyes, C. M.; Francisco, J. S.; Szente, J. J.; Maricq, M. M.; Ostergaard, L. F. Dimethyl Ether Oxidation at Elevated Temperatures (295−600 K). *J. Phys. Chem. A* **2005**, *109*, 10940−10953.
(17) Eskola, A. J.; Carr, S. A.; Blitz, M. A.; Pilling, M. J.; Seakins, P. W. Kinetics and Yields of OH Radical from the $CH_3OCH_2$ + $O_2$ Reaction Using a New Photolytic Source. *Chem. Phys. Lett.* **2010**, *487*, 45−50.
(18) Andersen, A.; Carter, E. A. First-Principles-Derived Kinetics of the Reactions Involved in Low-Temperature Dimethyl Ether Oxidation. *Mol. Phys.* **2008**, *106*, 367−396.
(19) Yamada, T.; Bozzelli, J. W.; Lay, T. H. Comparisons of CBS-Q and G2 Calculations on Thermodynamic Properties, Transition States, and Kinetics of Dimethyl-Ether Plus $O_2$ Reaction System. *Int. J. Chem. Kinet.* **2000**, *32*, 435−452.
(20) Skodje, R. T.; Tomlin, A. S.; Klippenstein, S. J.; Harding, L. B.; Davis, M. J. Theoretical Validation of Chemical Kinetic Mechanisms: Combustion of Methanol. *J. Phys. Chem. A* **2010**, *114*, 8286−8301.
(21) Turanyi, T.; Zalotai, L.; Dobe, S.; Berces, T. Effect of the Uncertainty of Kinetic and Thermodynamic Data on Methane Flame Simulation Results. *Phys. Chem. Chem. Phys.* **2002**, *4*, 2568−2578.
(22) Zador, J.; Zsely, I. G.; Turanyi, T. Local and Global Uncertainty Analysis of Complex Chemical Kinetic Systems. *Reliability Engineering & System Safety* **2006**, *91*, 1232−1240.
(23) Ziehn, T.; Hughes, K. J.; Griffiths, J. F.; Porter, R.; Tomlin, A. S. A Global Sensitivity Study of Cyclohexane Oxidation under Low Temperature Fuel-Rich Conditions Using HDMR Methods. *Combustion Theory and Modelling* **2009**, *13*, 589−605.
(24) Ziehn, T.; Tomlin, A. S. A Global Sensitivity Study of Sulfur Chemistry in a Premixed Methane Flame Model Using HDMR. *Int. J. Chem. Kinet.* **2008**, *40*, 742−753.
(25) Zsely, I. G.; Zador, J.; Turanyi, T. Uncertainty Analysis of NO Production During Methane Combustion. *Int. J. Chem. Kinet.* **2008**, *40*, 754−768.
(26) Bossmeyer, J.; Brauers, T.; Richter, C.; Rohrer, F.; Wegener, R.; Wahner, A. Simulation Chamber Studies on the $NO_3$ Chemistry of Atmospheric Aldehydes. *Geophys. Res. Lett.* **2006**, *33*, L18810.
(27) Carr, S. A.; Glowacki, D. R.; Liang, C. H.; Baeza-Romero, M. T.; Blitz, M. A.; Pilling, M. J.; Seakins, P. W. Experimental and Modeling Studies of the Pressure and Temperature Dependences of the Kinetics and the OH Yields in the Acetyl + $O_2$ Reaction. *J. Phys. Chem. A* **2011**, *115*, 1069−1085.
(28) Sharma, S.; Raman, S.; Green, W. H. Intramolecular Hydrogen Migration in Alkylperoxy and Hydroperoxyalkylperoxy Radicals: Accurate Treatment of Hindered Rotors. *J. Phys. Chem. A* **2010**, *114*, 5689−5701.
(29) Andersen, A.; Carter, E. A. Hybrid Density Functional Theory Predictions of Low-Temperature Dimethyl Ether Combustion Pathways. II. Chain-Branching Energetics and Possible Role of the Criegee Intermediate. *J. Phys. Chem. A* **2003**, *107*, 9463−9478.
(30) Suzaki, K.; Takahisa, C.; Tsuchiya, K.; Koshi, M.; Tezaki, A. Formation Pathways of $HO_2$ and OH Changing as a Function of Temperature in Photolytically Initiated Oxidation of Dimethyl Ether. *Proc. Combust. Inst.* **2007**, *31*, 295−303.
(31) Miller, W. H. Tunneling Corrections to Unimolecular Rate Constants, with Application to Formaldehyde. *J. Am. Chem. Soc.* **1979**, *101*, 6810−6814.
(32) Bartis, J. T.; Widom, B. Stochastic-Models of Interconversion of 3 or More Chemical Species. *J. Chem. Phys.* **1974**, *60*, 3474−3482.
(33) Sobol, I. On the Distribution of Points in a Cube and the Approximation Evaluation of Each Integrals. *Comp Math Math Phys.* **1976**, *7*, 86−112.
(34) Ziehn, T.; Tomlin, A. S. Gui-HDMR - a Software Tool for Global Sensitivity Analysis of Complex Models. *Environmental Modelling & Software* **2009**, *24*, 775−785.
(35) Holbrook, K. A.; Pilling, M. J.; Robertson, S. H.; Robinson, P. J. *Unimolecular Reactions*, 2nd ed.; Wiley: Chichester ; New York, 1996.
(36) Rabitz, H.; Alis, O. F.; Shorter, J.; Shim, K. Efficient Input-Output Model Representations. *Comput. Phys. Commun.* **1999**, *117*, 11−20.
(37) Li, G. Y.; Wang, S. W.; Rabitz, H.; Wang, S. Y.; Jaffe, P. Global Uncertainty Assessments by High Dimensional Model Representations (HDMR). *Chem. Eng. Sci.* **2002**, *57*, 4445−4460.
(38) Kucherenko, S.; Tarantola, S.; Annoni, P. Estimation of Global Sensitivity Indices for Models with Dependent Variables. *Comput. Phys. Commun.* **2012**, *183*, 937−946.
(39) Nagy, T.; Turanyi, T. Reduction of Very Large Reaction Mechanisms Using Methods Based on Simulation Error Minimization. *Combust. Flame* **2009**, *156*, 417−428.
(40) Mara, T. A.; Tarantola, S. Variance-Based Sensitivity Indices for Models with Dependent Inputs. *Reliability Engineering & System Safety* **2012**, *107*, 115−121.
(41) Nagy, T.; Turányi, T. Uncertainty of Arrhenius Parameters. *Int. J. Chem. Kinet.* **2011**, *43*, 359−378.
(42) Nagy, T.; Turányi, T. Determination of the Uncertainty Domain of the Arrhenius Parameters Needed for the Investigation of Combustion Kinetic Models. *Reliability Engineering & System Safety* **2012**, *107*, 29−34.
(43) Turányi, T.; Nagy, T.; Zsely, I. G.; Cserhati, M.; Varga, T.; Szabo, B. T.; Sedyo, I.; Kiss, P. T.; Zempleni, A.; Curran, H. J. Determination of Rate Parameters Based on Both Direct and Indirect Measurements. *Int. J. Chem. Kinet.* **2012**, *44*, 284−302.
(44) Tomlin, A. S.; Agbro, E.; Nevrly, V.; Dlabka, J.; Vasinek, M. Evaluation of Combustion Mechanisms Using Global Uncertainty and Sensitivity Analyses: A Case Study for Low-Temperature Dimethyl Ether Oxidation. *Int. J. Chem. Kinet.* **2014**, *46*, 662−682.


DOI: 10.1021/acs.jpca.5b00620
*J. Phys. Chem. A* XXXX, XXX, XXX−XXX